Modeling nonlinear dynamics of CAM productivity and water use for global predictions

Samantha Hartzell[1], Mark S. Bartlett[2,3], Paolo Inglese[4], Simona Consoli[5], Jun Yin[6], Amilcare Porporato[7,8,*]

*Corresponding Author: Amilcare Porporato

Department of Civil and Environmental Engineering

Princeton Environmental Institute

Princeton University

E-208 E-Quad, Princeton, NJ 08540 U.S.A.

Phone +1 609 258 2287

e-mail aporpora@princeton.edu

[1]Department of Civil and Environmental Engineering, Portland State University

[2]Stantec

[3]Department of Civil and Environmental Engineering, Duke University

[4]Dipartimento di Scienze Agrarie, Alimentari e Forestali, Università degli Studi di Palermo

[5]Dipartimento di Agricoltura, Alimentazione e Ambiente, Università degli Studi di Catania

[6]School of Hydrology and Water Resources Engineering, Nanjing University of Information Science and Technology

[7]Department of Civil and Environmental Engineering, Princeton University

[8]Princeton Environmental Institute, Princeton University

Funding

This work was supported through the USDA Agricultural Research Service cooperative agreement 58-6408-3-027 and National Institute of Food and Agriculture (NIFA) grant 12110061; National Science Foundation (NSF) grants EAR-1331846, FESD- 1338694, EAR-1316258, and GRFP-1106401; the Carbon Mitigation Initiative (CMI) at Princeton University; the AFRI Postdoctoral Fellowship program Grant No. 2017-67012-26106/Project Accession No. 1011029 from the USDA National Institute of Food and Agriculture; and the National Natural Science Foundation of China (41877158, 51739009).

Abstract

Crassulacean acid metabolism (CAM) crops are important agricultural commodities in water-limited environments across the globe, yet modeling of CAM productivity lacks the sophistication of widely used C3 and C4 crop models, in part due to the complex responses of the CAM cycle to environmental conditions. This work builds on recent advances in CAM modeling to provide a framework for estimating CAM biomass yield and water use efficiency from basic principles. These advances, which integrate the CAM circadian rhythm with established models of carbon fixation, stomatal conductance, and the soil-plant-atmosphere continuum, are coupled to models of light attenuation, plant respiration, and biomass partitioning. Resulting biomass yield and transpiration for *Opuntia ficus-indica* and *Agave tequilana* are validated against field data and compared with predictions of CAM productivity obtained using the empirically-based Environmental Productivity Index (EPI). By representing regulation of the circadian state as a nonlinear oscillator, the modeling approach captures the diurnal dynamics of CAM stomatal conductance, allowing the prediction of CAM transpiration

and water use efficiency for the first time at the plot scale. This approach may improve estimates of CAM productivity under light-limiting conditions when compared with previous methods.

Keywords: Crassulacean acid metabolism, carbon assimilation, water use efficiency, biomass, *Opuntia ficus-indica*, *Agave tequilana*

Running head: Nonlinear CAM dynamics for global predictions

1. Introduction

Due to their unique circadian rhythm of nocturnal carbon dioxide uptake and storage, CAM photosynthetic plants regularly achieve a water use efficiency six or more times higher than that of their C3 counterparts (Lambers, Stuart Chapin III, & Pons, 2008), making them promising candidates for food, fodder, and biofuel production in water-stressed ecosystems across the globe. In particular, cactus pear (*Opunita ficus-indica*) and many species of agaves, including *Agave tequilana*, *Agave fourcroydes*, and *Agave deserti*, are important sources of human nutrition, animal forage, and fiber production, in Mexico, South America, and Northern Africa, among other locations. Recent research has set out to answer questions about the potential of these crops for biofuel production and food security in future warming and drying environments (Borland et al., 2009; de Cortazar & Nobel, 1990; Mason et al., 2015; Owen & Griffiths, 2014; Yang et al., 2015).

In support of these efforts, a number of modeling approaches have arisen to represent CAM plants at varying levels of complexity. Such approaches may be broadly grouped into empirical descriptions of CAM productivity (Niechayev et al., 2018; Nobel, 1988), process-based models which incorporate simplified mathematical representations of the CAM circadian rhythm (Bartlett et al., 2014; Blasius et al., 1999; Hartzell et al., 2018), and detailed biochemical approaches (Owen & Griffiths, 2013; Shameer et al., 2018). The environmental productivity index (EPI) is an empirical method which multiplicatively combines functions of solar radiation, temperature, and soil moisture to predict CAM dry mass productivity at the monthly timescale (Nobel 1988). It was developed and parameterized to predict productivity of *Opuntia ficus-*

indica, *Ferocactus acanthodes*, and many species of agaves in the Southwestern U.S., Mexico, and Chile, sites which tend to be exposed to high levels of photosynthetically active radiation (PAR) during the main growing season (Niechayev et al., 2018; Nobel, 1985; Nobel & Hartsock, 1986; Nobel & Meyer, 1985; Nobel & Quero, 1986; Nobel & Valenzuela, 1987). Thus far, it has been the only method of estimating CAM productivity at the plot scale and over the course of a growing season. The modeling approach introduced by Bartlett et al. (2014) and incorporated in the Photo3 model (Hartzell et al., 2018) couples a mathematical representation of the CAM circadian rhythm as a Van der Pol oscillator with established models of carbon fixation (Farquhar et al., 1980), stomatal conductance (Katul & Oren, 2009; Medlyn et al., 2011), and the soil-plant-atmosphere continuum to calculate CAM carbon assimilation and transpiration on an hourly timescale and at the plant scale based upon PAR, temperature, specific humidity, and soil moisture, but does not address resource allocation or dry mass productivity.

The goal of this work is to determine whether this representation of the CAM process may shed light on the productivity of CAM crops under field conditions. To do so, we couple the described modeling approach with process-based representations of light attenuation, plant respiration, and biomass partitioning in order to calculate biomass yield and water use efficiency in the CAM crops *Agave tequilana* and *Opuntia ficus-indica*. Unlike previous techniques, this modeling approach takes into account vapor pressure deficit, daytime temperature, and diurnal fluctuations of environmental conditions, which have been shown to be important factors in CAM productivity and water use efficiency (Conde & Kramer, 2008; Hartzell et al., 2015; Kluge & Ting, 1978; Wilkins, 1992). Model results are compared directly with field data from the Americas and the Mediterranean (Consoli et al., 2013; de Cortazar et al. ,1985; Nobel &

Valenzuela, 1987), and with EPI predictions. The productivity estimates agree with field data obtained across a range of environmental conditions. This approach is the first to provide validated estimates of long-term water use by CAM plants at the plot scale. Results show that CAM productivity and water use can be successfully described using a process-based model of CAM photosynthesis and hydraulics. The findings allow direct comparison of CAM productivity and water use with C3 and C4 crops, contributing to the understanding of CAM potential in global agriculture.

2. Materials and methods

2.1. Modeling net carbon assimilation and transpiration

The CAM carbon and water fluxes are modeled according to the Photo3 model (Hartzell et al., 2018). CAM photosynthesis is described using a circadian rhythm oscillator which depicts malic acid storage and release, with CO_2 demand by the Calvin cycle (A_c) modeled according to Farquhar et al. (1980) (see Fig. 1). The carbon demand of the Calvin cycle is given by the Farquhar et al. (1980) model with modifications to account for water and nutrient stress, i.e.,

$$A_c(\phi, c_i, T_l, \psi_l) = A_{\phi,c_i,T_l}(\phi, c_i, T_l) \cdot f_{\psi_l}(\psi_l) \cdot f_n, \qquad (1)$$

where A_{ϕ,c_i,T_l} is a function of solar radiation, ϕ, internal CO_2 concentration, c_i, and leaf temperature, T_l, given according to (Farquhar et al., 1980), and f_{ψ_l} is a piecewise function of leaf water potential, ψ_l, which decreases carbon assimilation at low leaf water potential (Daly et al.

123 2004). Where applicable, soil nutrient limitations are assumed to reduce the carbon demand
124 through a dimensionless nutrient limitation factor, f_n, which is equal to 1 in cases for which
125 nutrients are non-limiting. This assumption is supported by observations that soil nitrogen
126 availability is linearly related to leaf nitrogen concentration in *O. ficus-indica* (Dubeux et al.,
127 2006). Leaf nutrient availability in turn directly affects photosynthetic potential through a
128 number of mechanisms, including the maximum photosynthetic rate and the stomatal
129 conductance (Morales et al., 2018).
130
131 The various carbon fluxes, from the stomata to the Calvin cycle (A_{sc}), from the stomata to the
132 cell vacuole (A_{sv}), and from the cell vacuole to the Calvin cycle (A_{vc}), depend on the carbon
133 demand at the Calvin cycle (A_c) and are regulated by two state variables: the malic acid
134 concentration (M), and the circadian rhythm order (z) (Bartlett et al., 2014). The timing of these
135 state variables is regulated by a system of coupled differential equations which form a nonlinear
136 oscillator. The carbon demand at the stomata (A_n) is the sum of the carbon flux from the stomata
137 to the Calvin cycle (A_{sc}) in Phase II and IV of CAM, and that from the stomata to malic acid
138 storage (A_{sv}) in Phase I of CAM, which are, in turn, functions of environmental conditions
139 (Bartlett et al., 2014; Hartzell et al., 2015), i.e.,
140

$$A_n(\phi, c_i, T_l, \psi_l, z, M) = A_{sc}(\phi, c_i, T_l, \psi_l, z, M) + A_{sv}(T_l, \psi_l, z, M). \quad (2)$$

141 The diurnal cycle of uptake and release from the vacuole is represented by a pair of balance
142 equations for M and z. The balance equation for the malic acid concentration is given by
143

$$L_M \frac{dM}{dt} = A_{sv}(T_l, \psi_l, z, M) + R_{dv}(T_l, \psi_l) - A_{vc}(\psi_l, c_c, T_l z, M), \quad (3)$$

where L_M is the ratio of malic acid storage volume to the C flux surface area, c_c is the increased internal CO_2 concentration due to malic acid decarboxylation (Bartlett et al., 2014), R_{dv} is the portion of respiratory carbon refixed as malic acid in the vacuole, and A_{vc} is the flux of carbon from the cell vacuole to the Calvin cycle in Phase III of CAM . The circadian rhythm order is given by

$$t_r \frac{dz}{dt} = \frac{M - M_E(z, T_l),}{M_{max}} \quad (3)$$

where t_r is the relaxation time, M_E is the equilibrium concentration of malic acid, and M_{max} is the maximum malic acid concentration. The details of each of the involved expressions are presented in full in Hartzell et al. (2018). When coupled with the model of carbon demand at the Calvin cycle A_c (Eq. 1), the nonlinear oscillator produced by the system of equations for M and z (Eq. 3, 4) results in simulated carbon uptake at the stomata (A_n) (Eq. 2).

Stomatal conductance of C3 and C4 plants can be assumed to act to minimize the amount of water used per unit carbon gained, an assumption that leads to the stomatal conductance scaling with the carbon demand A_n and with the square root of the vapor pressure deficit D (Katul et al., 2009; Medlyn et al., 2011; Oren et al., 1999). CAM plants are typically under strong pressure to maximize water use efficiency (Winter & Smith, 1996) and have been shown to respond directly to changes in ambient humidity (Lange & Medina, 1979; Males & Griffiths, 2017; Osmond et al., 1979). Therefore, they are assumed to follow such an optimization principle, i.e.,

$$g_{s,CO_2} = \frac{g_1 A_n}{c_a \sqrt{D}}, \quad (4)$$

where c_a is the atmospheric CO_2 concentration and g_1 is a dimensionless factor which is often fitted empirically to data, with an average value of 3.5 for C3 plants (Leuning, 1995). Following the assumption of Fickian diffusion through the stomata, it can be shown that such a factor should be related to the observed ratio of internal to atmospheric CO_2 ($R = c_i/c_a$) such that $g_1 = (1 - R)^{-1}$ (Bartlett et al., 2014; Norman, 1982). The value of R has been reported, on average, to be significantly higher for C3 (~0.7) than for CAM plants (~0.5) (Jones 2014, p. 159). Given this relationship, a typical value of g_1 for CAM photosynthesis would be expected to be somewhat less than the value for C3 photosynthesis. We use a value of 2.8, which matches estimates of daytime CO_2 assimilation rates in partial or facultative CAM plants (see Fig. 2d and Hartzell et al. (2018)).

The leaf level respiration, R_d, is represented as a temperature-dependent process which follows a modified Arrhenius equation (Bartlett et al., 2014; Hartzell et al., 2018). Respired CO_2 may be directly refixed through the Calvin cycle through the flux R_{dc} or fixed as malic acid in the cell vacole through the flux R_{dv} (see Figure 1), where this partitioning is dependent on incident solar radiation levels (see Appendix 1 of Bartlett et al. (2014). This depiction allows for CAM cycling (nocturnal recycling of respiratory carbon) and CAM idling (respiratory carbon being refixed during periods when stomata are closed throughout the night and day).

183 The hydraulic fluxes through the plant and the leaf water potential are modeled through a
184 resistor-capacitor analog model which accounts for plant water storage to calculate the impact of
185 water stress based on soil and atmospheric conditions, accounting for the role of previous soil
186 moisture history on current plant water status (see Figure 1). For model simplicity, we assume a
187 constant plant hydraulic capacitance (see Table 1). The hydraulic conductances between the
188 plant and soil, g_{sr}, the transpiration stream and stored water, g_w, and the plant hydraulic
189 conductance, g_p, are functions of water potential as described in Hartzell et al. (2018), Appendix
190 B.
191
192 The full model equations, as well as photosynthetic and hydraulic parameters for *O. ficus-indica*,
193 are described in Hartzell et al. (2018) and are used here with one modification: the quantum
194 yield, κ_2 (dimensionless), has been adjusted to a value of 0.1 following Nobel and Hartsock
195 (1983) and Skillman (2008) to better represent knowledge of CAM efficiency (see Fig. 2a,b).
196 The primary photosynthetic parameters (the maximum electron transport rate $V_{c,max}$, which
197 controls the maximum permitted rate of carbon fixation in the Calvin cycle; the maximum malic
198 acid concentration M_{max}, which controls the maximum amount of carbon fixation as malic acid
199 in Phase I; and the maximum malic acid storage flux $A_{m,max}$, which controls the maximum
200 carbon flux from the stomata to the cell vacuole) have been fitted based on diurnal gas exchange
201 data for the two species of interest, *A. tequilana* and *O. ficus-indica* (see Table 1, Figure 2c,d).
202 While the maximum rate of CO_2 uptake for the two species is similar, the differences in daytime
203 CO_2 uptake are reflected in the parameters M_{max} and $A_{m,max}$, such that under well-watered
204 conditions the carbon demand of *A. tequilana* may not be fully met by stored malic acid, and
205 stomata may open in the second half of the light period (Nobel & Valenzuela, 1987; Owen et al.,

206 2016). The typical stem area index (SAI) is given in Table 1 and is modified for the various
207 scenarios described in "*2.6. Model validation*." The complete model with these updates is
208 available online at GitHub (https://github.com/samhartz/Photo3).
209
210 2.2. Calculation of the Environmental Productivity Index
211
212 We calculate the EPI using the methodology outlined in Nobel and Hartsock (1986) and Nobel
213 and Valenzuela (1987) for *O. ficus-indica* and *A. tequilana*. Temperature, light, and soil moisture
214 indices are calculated at a monthly timescale and multiplied by the maximal productivity to
215 obtain the estimated aboveground dry mass productivity. The temperature index is calculated
216 according to the average minimum daily temperature, the light index is a function of monthly
217 average total daily photosynthetically active radiation (PAR), and the water stress index is a
218 function of drought duration, being equal to one until the soil water potential has dropped below
219 a threshold value for a certain number of days, at which point it begins to decrease. Parameters
220 for each of the indices have been determined empirically and may be found in Nobel and
221 Hartsock (1986).
222
223 2.3. PAR interception
224
225 Numerous difficulties exist when modeling interception of photosynthetically active radiation
226 (PAR) in CAM plants. Rather than possessing semi-translucent and mobile canopies as is typical
227 of most crops, CAM crops such as *Opuntia* sp. and *Agave* sp. photosynthesize through stems
228 which are almost entirely opaque and non-mobile. This means that one cannot assume that the

incident PAR is felt by the entire stem surface. In addition, not all stem area can be assumed to be photosynthetically active; in *Opuntia* sp., 20-40% of the stem area is lignified and does not contribute significantly to photosynthesis (Inglese et al. 2012). Efforts have been made to understand the effect of shading in CAM plants (de Cortazar et al., 1985; Geller & Nobel, 1987) but to date have not been generalized.

We address this problem by calculating a general index of PAR interception for *Agave* sp. and *Opuntia* sp. based on measured cladode distribution and PAR attenuation. Data from de Cortazar et al. (1985) gives vertical distributions of stem area index (SAI) and light attenuation for *O. ficus-indica* (see Fig. 3). These observations are used to calculate an overall PAR interception factor of 0.58 by multiplying the incident PAR (Fig. 3b) by the fractional photosynthetically active cladode area at each canopy layer (Fig. 3a) and summing over the distribution of canopy layers shown in Fig. 3c. This calculation assumes that the bottom 30% of stem area is lignified and does not contribute to photosynthesis (Liguori et al. 2014). In *Agave* sp., PAR distribution across the photosynthetically active surface has been found to be relatively uniform (Nobel 1985). Woodhouse et al. (1980) showed that total PAR averaged on leaf surfaces of *Agave deserti* was about 33% of incoming PAR in summer, and 37% in winter. Nobel (1985) found that the PAR distribution across *Agave fourcroydes* was approximately 28% of incoming PAR. Based on this data we assumed a PAR interception factor of 0.3 for *Agave* sp.

Previous work supports the notion that a fully resolved 3-dimensional model of light interception based on cladode positions produces results consistent with models developed using statistical averages of light attenuation (de Cortazar et al., 1985). This approach, while a simplification,

252 eliminates the need to calculate light attenuation based on canopy geometry which is often
253 prohibitive for general studies. The incoming PAR (ϕ) used in the calculations of carbon
254 assimilation is multiplied by the calculated PAR interception factor (f_l) to account for light
255 interception.
256
257 2.4. Biomass partitioning
258
259 We assume that plants are at the mature stage and that biomass is partitioned into four carbon
260 pools: leaves (or non-lignified, photosynthetically active cladodes), stems (or lignified, non-
261 photosynthetically active cladodes), roots, and storage (reproductive) organs. Although
262 partitioning ratios between the pools may change seasonally, we assume average partitioning
263 ratios determined by the total biomass accumulation over the course of the growing season (see
264 Table 1).
265
266 The change in total biomass B is given by the net carbon assimilation A_n (this accounts for leaf
267 respiration) less the root respiration R_r and growth respiration, R_g, i.e.,
268

$$\frac{dB}{dt} = A_n - R_r - R_g. \qquad (5)$$

269 This total biomass production is then divided into the four carbon storage pools, leaf biomass B_l
270 (for *Opuntia* sp. defined as green or unlignified stem), stem biomass B_s (for *Opuntia* sp. defined
271 as lignified stem), root biomass B_r, and storage biomass B_o (for *Opuntia* sp. defined as fruit).
272

273 The growth of root biomass, B_r, is directly related to the total biomass growth as

274

$$\frac{dB_r}{dt} = r_r \frac{dB}{dt}, \quad (6)$$

275 where r_r is the ratio of root to total biomass allocation. Similarly, the growth of leaf biomass, B_l

276 is given by

$$\frac{dB_l}{dt} = r_l(1 - r_r) \frac{dB}{dt}, \quad (7)$$

277 where r_l is the ratio of leaf to total aboveground biomass allocation. Stem biomass B_s and

278 storage organ biomass B_o are calculated in the same manner using the ratios r_s and r_o,

279 respectively (see Table 1). The mass of carbon fixed is converted to dry biomass using a factor of

280 27 g dry weight plant material per mol carbon fixed (Cui et al., 1993; Liguori et al., 2014; Nobel

281 & Hartsock, 1986).

282

283 2.5. Respiration

284

285 Carbon dioxide produced by respiration in CAM can be refixed both in the light (via the Calvin

286 Cycle) and in the dark (via phosphoenolpyruvate carboxylase (PEPC) fixation). Thus, it is not

287 possible to measure directly via typical gas exchange systems. This has resulted in a dearth of

288 information regarding growth and maintenance respiration of aboveground CAM biomass

289 (Tcherkez, 2017). In this model, the leaf respiration is accounted for in the net carbon

assimilation A_n. Growth respiration is assumed to be a constant fraction of the net carbon assimilation as observed in C3 and C4 photosynthetic plants (Amthor, 1994):

$$R_g(A_n) = \eta_g \cdot A_n, \quad (8)$$

where η_g is the growth respiration coefficient (Weng et al., 2014).

The root maintenance respiration is given following Weng et al. (2014), with modifications to account for water stress, as:

$$R_r = \beta_r \cdot f_A(T_l) \cdot f_T(T_l) \cdot f_{\psi_l}(\psi_l) \cdot B_r, \quad (9)$$

where T_l is the leaf temperature, B_r is the biomass of the roots, and β_r is the root respiration coefficient, equal to 1.25 yr^{-1}. The respiration is affected by temperature through a modified Arrhenius function, f_A, following Leuning (1995),

$$f_A(T_l) = \exp\big(k \cdot (1/T_0 - 1/T_l)\big), \quad (10)$$

where k = 3000 and T_0 is a reference temperature of 288 K; and by a thermal inhibition function, f_T, given by

$$f_T(T_l) = \Big(\big(1 + \exp\big(0.4 \cdot (T_L - T_l)\big)\big) \cdot \big(1 + \exp\big(0.4 \cdot (T_l - T_H)\big)\big)\Big)^{-1}, \quad (11)$$

where T_L and T_H are the low and high temperatures below and above which respiration is limited. Finally, respiration is a product of the water stress function $f_{\psi_l}(\psi_l)$ given in Eq. (1) (as supported by Palta and Nobel (1989)).

2.6. Model validation

Model results were compared with established productivity validated in the field and with results obtained using the EPI method. Aboveground biomass accumulation for *O. ficus-indica* in central Chile was compared with data collected from May 1980-August 1981 in Til Til, Chile by de Cortazar et al. (1985) for a stem area index (SAI) of 1.4 in loamy sand. Solar radiation, specific humidity, and air temperature from May 2012-August 2013 from the La Platina station of the Chilean Institute of Agricultural Research (INIA) Agromet network were selected as model inputs since this period included neither El Niño nor La Niña conditions in accordance with the original study period (see Fig. 4a-c) and recalculation of the EPI using this data produced results similar to the original EPI calculations (see Supporting Information Figure S4). The productivity was calculated assuming well-watered conditions and results were adjusted by the EPI water index to facilitate comparison with field results.

Model results were also compared with measurements of productivity and transpiration for *O. ficus-indica* in Southern Italy obtained by Consoli et al. (2013) for ten-year-old plants with a stem area index (SAI) of 3.5 and full irrigation in clay-loam soil. Aboveground dry mass productivity per unit leaf area was converted to productivity per unit plot area by multiplying by the SAI (3.5) and by a factor to account for the percentage of land covered by cactus canopy (0.65). Hourly environmental data (solar radiation, temperature, and humidity) collected during the original study, which took place in Roccapalumba, Italy from June - November 2009, were

used as inputs to the model (see Fig. 4g-i). In accordance with soil moisture measurements, the soil moisture was assumed to be non-limiting (equal to the field capacity) for the simulation.

Model results for *A. tequilana* were compared with results from a field experiment in Jalisco, Mexico collected by Nobel and Valenzuela (1987) for plants initially six years old with a leaf area index of 6. Because nutrient limitation appears to have been significant in the Nobel and Valenzuela (1987) study (the typical daily PAR levels of 30-50 mol m^{-2} d^{-1} were well above levels of 20 mol m^{-2} d^{-1} used to calculate maximum productivity rates in laboratory experiments), data from an independent study of *A. tequilana* productivity in Jalisco, Mexico (Nobel 1989) were used to estimate the nutrient limitation factor, f_n. The annual rates of leaf unfolding for 1-year-old and 3-year-old plants at the site (approximately 23 and 35 leaves per year, respectively) were compared with annual rates of leaf unfolding for 2-year-old plants grown in Jalisco, Mexico in a study of nutrient effect on *A. tequilana* productivity (Nobel 1989). The study showed a strong linear relationship between leaf unfolding rates and nutrient limitation. Based on this relationship, a leaf unfolding rate of 29 leaves yr^{-1} for 2-year old plants (selected based on an interpolation of leaf unfolding rates vs. age for the three age groups presented in Nobel and Valenzuela (1987) corresponded with a nutrient index of 0.4. The productivity and water use were calculated using solar radiation, specific humidity, and temperature data obtained from the NSRDB database from Jalisco, Mexico during the period April 2001 until April 2002, the earliest availability of high temporal resolution data which included neither El Niño nor La Niña conditions similarly to the study period (see Fig. 4d-f). Average temperature and solar radiation values closely matched the monthly data recorded from the study period (see Nobel and Valenzuela (1987)). Daily rainfall data from the nearby Santa Rosa site were obtained from the

Mexican National Meteorological Service Climate Computing project (CLICOM) for the original study period and were used to simulate soil moisture.

2.7. Productivity predictions

The aboveground biomass productivity of *Opuntia ficus-indica* was estimated using both the described modeling approach and the EPI for the six regions worldwide with the highest production of *Opuntia* sp. as estimated by the Food and Agriculture Organization (Inglese et al., 2017). These regions included Northeast Brazil, Central Mexico, Northern Ethiopia, Western Morocco, Southern Italy, and Central Chile. Unless otherwise noted, climate data including soil moisture were obtained from CERA-20 C reanalysis data (European Center for Medium-Range Weather Forecasts). For all simulations, a uniform stem area index of 3.5 was assumed (see *Supporting information* for more details). To evaluate the impact of various rainfall regimes and the potential of irrigation in each region, productivity estimates for each method were calculated under both rainfed conditions (using local soil moisture data) and well-watered conditions (assuming a constant volumetric soil moisture of 0.7).

3. Results

3.1 Model results for carbon exchange at the hourly timescale

Model results for *O. ficus-indica* captured Phases I and III of the observed behavior and suggested a short Phase II and IV uptake of CO_2 which have been observed for *O. ficus-indica* under similar conditions (Cui & Nobel, 1994; Cui et al., 1993) but were not present in this

particular dataset (Fig. 2c). Due to the assumption of a fixed t_r (Eq. 4), the model underestimated the rate of decrease of carbon uptake occurring at the end of Phase I for this dataset.

Results for *A. tequilana* captured all four phases of CAM, with a high nocturnal Phase I uptake of CO_2, a short Phase II uptake at the start of the light period, and a moderate uptake of CO_2 during the second half of the light period in Phase IV (Fig. 2d). The model failed to capture the decline of CO_2 assimilation to zero at the end of the light period (Nobel & Valenzuela, 1987), and represented a continuous transition between the end of Phase III and the onset of Phase IV. In this scenario, the model overestimated the rate of decrease of carbon uptake at the end of Phase I, again due to assuming a fixed t_r.

3.2. Model results for biomass accumulation and transpiration at the monthly timescale

3.2.1. Opuntia ficus-indica

Validation of model results for *O. ficus-indica* are performed for sites in Til Til, Chile and Sicily, Italy. Til Til, Chile exhibits strong climate seasonality, with very high solar radiation during the primary growing season in the summer (average of 50-60 mol m^{-2} daily total PAR), relatively low vapor pressure deficit, and favorable temperatures ranging from 10-30 C during the summer (see Fig. 4a-c). The total annual dry weight gain on a stem area basis from May 1980-May 1981 estimated by the Photo3 model is 1.3 kg m^{-2} yr^{-1}, while the measured value is 1.2 kg m^{-2} yr^{-1} , and the EPI estimate is 1.0 kg m^{-2} yr^{-1} (de Cortazar et al., 1985) (see Fig. 5a). On a month-to-month

396 basis, the EPI predictions are similar to the Photo3 predictions, particularly during the summer.
397 During the winter period of May, June, and July 1980, the Photo3 estimates of dry weight gain
398 are consistently higher than those of the EPI, by about 25%. Calculated total annual transpiration
399 is 321 mm, average daily transpiration is 0.71 mm d^{-1}, and average daily transpiration during the
400 principal growing season (Jan-Mar) is 1.3 mm d^{-1} (Fig. 5b). This results in an annual average
401 water use efficiency of 4.0 g DM kg^{-1} H_2O.
402
403 The Sicily, Italy site is characterized by relatively low solar radiation, high daytime temperature,
404 and high daytime vapor pressure deficit (see Fig. 4d-f). Although the majority of rainfall was
405 concentrated outside the main growing period, irrigation was provided to the site such that soil
406 moisture did not impact productivity. Rather, low PAR was the primary limiting factor. Results
407 from the Photo3 model and from the EPI are compared with productivity results from Consoli et
408 al. (2013), which measured an aboveground dry mass productivity of 1.29 kg m^{-2} over the course
409 of the growing season. Productivity results from the Photo3 model (1.30 kg m^{-2} plot area) are
410 very close to the study results, and results from the EPI model (0.89 kg m^{-2} plot area) are about
411 30% lower than the study results (see Fig. 5c). Daily transpiration calculated by the Photo3
412 model during the study period is shown in Fig. 5d. Estimated average daily transpiration is 1.4
413 mm d^{-1}. The total transpiration calculated on a plot area from the months June-September is 162
414 mm, while the measured transpiration was estimated from eddy covariance measurements to be
415 204 mm over the same time period. To maintain consistency with the Consoli (2013) study, the
416 transpiration water use efficiency is calculated using the dry matter accumulation during the
417 period June-November, and the transpiration during the period June-September. This resulted in

418 an estimated transpiration WUE 8.0 g DM kg^{-1} H_2O, while measured transpiration water use
419 efficiency was 6.3 g DM kg^{-1} H_2O (Consoli et al., 2013).
420
421 *3.2.2. Agave tequilana*
422
423 5,000 ha in Mexico are under cultivation of *Agave tequilana*, with more than 99% concentrated
424 in the state of Jalisco due to its protected status and the region's favorable growing conditions
425 (Iñiguez-Covarrubias et al., 2001). The region of Jalisco is characterized by very high solar
426 radiation, relatively low vapor pressure deficit, and favorable temperatures during the primary
427 growing season of June-November (see Fig. 4g-i). As the crops were rainfed and the vast
428 majority (>99%) of the 1082 mm of annual rainfall occurred during the period June-November,
429 water was practically non-limiting during this period, while outside of this period soil moisture
430 was highly limiting. Main limiting factors appeared to be soil moisture and soil nutrient levels.
431 With a nutrient index of 0.4 the estimated productivity was 1.92 kg m^{-2} yr^{-1} on a ground area
432 basis, which was 9% lower than measured productivity at the site, 2.11 kg m^{-2} yr^{-1} (Fig. 6a). The
433 estimated EPI productivity, using a maximum net assimilation rate of 283.5 g m^{-2} $month^{-1}$, was
434 2.4 kg m^{-2} ground area during the study period (Nobel and Valenzuela 1987). The total
435 estimated transpiration over the study period was 87 mm per unit ground area with an average
436 daily transpiration of 0.24 mm d^{-1} during the course of the year and 0.37 mm d^{-1} during the
437 course of the growing season (Fig. 6b). The transpiration water use efficiency was 21.8 g DM kg^{-1}
438 H_2O. Soil moisture s and plant water storage content w were simulated using available rainfall
439 data, and both indicators demonstrated a strong seasonality, with volumetric soil moisture values
440 ranging from 20-25% during the dry season and 60-80% during the wet season (Fig. 6c) and

441 plant water content ranging from 18-25% during the dry season and 98-99% during the wet
442 season (Fig. 6d). Estimated plant water content reached lower values than those typically
443 observed in the field (about 30-40% according to Nobel & Jordan, 1983) due to a model
444 simplification assuming linear pressure-volume relations (Hartzell et al., 2018). This should not
445 significantly affect the predicted transpiration and carbon assimilation since neither occur in
446 model results when plant water status is below 30%.
447
448 3.3. Worldwide productivity prediction
449
450 *Opuntia* sp. is grown in drylands worldwide with the largest areas of cultivation estimated to
451 occur in Northeast Brazil, Central Mexico, Northern Ethiopia, Western Morocco, Southern Italy,
452 and Central Chile (Inglese et al., 2017). While the EPI has been tested and parameterized in
453 some of these locations (Mexico and Chile), others remain understudied in terms of productivity.
454 In the Western Hemisphere, predictions of biomass productivity derived using the described
455 method were generally similar to those calculated using the EPI (Figs. 7, S1, S2). In the Eastern
456 Hemisphere, however, results diverged significantly (Fig. 7a). Under well-watered conditions
457 expected productivity in Southern Italy was 2.3 kg m^{-2} yr^{-1} on a ground area basis, while that
458 obtained by the EPI model was 1.4 kg m^{-2} yr^{-1} (Fig. 7b). Results in Northern Africa diverged as
459 well: in Mekele, Ethiopia predicted productivity values from this method and the EPI model
460 were 6.4 and 4.6 kg m^{-2} yr^{-1} , respectively, and in Agadir, Morocco predicted productivity values
461 were 5.3 and 4.0 kg m^{-2} yr^{-1} , respectively. Reported values in these regions thus far are well
462 below the numbers predicted by either method (Arba et al., 2002; Arba et al., 2017; Boujghagh
463 & Bouharroud, 2015; Gebretsadik et al., 2013), suggesting that significant gains in yield may be

achieved through fertilization and increasing planting density in these areas. In Northeast Brazil, yields predicted by the two methods were similar and were well above reported values in the region, which averaged 0.7 kg m^{-2} yr^{-1} and showed very high variability (Menezes et al., 2005). It has been demonstrated that potential productivity in the region is significantly higher and yields of 2 kg m^{-2} yr^{-1} have been achieved by the Pernambuco Agricultural Research Agency (Menezes et al., 2005). These results suggest that, under optimal planting density and fertilization, current yields could potentially be doubled.

The areas in which the Photo3 model predicted a significantly higher productivity than the EPI model were characterized by a lower average solar radiation during the growing season in all three regions (Fig. S1). In Southern Italy, the average daily PAR during the most productive portion of the growing season was 30-40 mol m^{-2} d^{-1}, which decreased to below 20 mol m^{-2} d^{-1} in the final portion of the growing season (Fig. 4e). Likewise, in Ethiopia the average daily PAR was near 40 mol m^{-2} d^{-1} throughout the year, and in Morocco, the PAR ranged from 20-30 mol m^{-2} d^{-1} during the rainy season (Fig. S1). In the sites in the Western Hemisphere, on the other hand, the PAR ranged from 50-65 mol m^{-2} d^{-1} during the growing season (Figs. 4b,h, S1). Under rainfed conditions (Fig. 7c), in areas where water stress affected the model results it often had a stronger negative effect on the Photo3 estimates than on the EPI estimates, as is seen in the predictions for Mexico, Italy, and Morocco. All three of these locations were characterized by small, intermittent rainfall events during the growing season (Fig. S1, S3).

4. Discussion

The modeling approach outlined in this work enables the prediction of CAM productivity and water use under a diverse set of field conditions using established relationships of plant physiology and basic CAM modeling, enabling a better understanding of CAM potential and environmental feedbacks worldwide. While many details of CAM metabolism and signaling are still under active investigation (Shameer et al., 2018), portrayal of the CAM circadian rhythm as a nonlinear oscillator allows biomass accumulation and water use by the CAM crops *Agave tequilana* and *Opuntia ficus-indica* to be understood under field conditions. This study represents the first predictions of CAM biomass productivity using a process-based model, and the first validated model predictions of long-term CAM transpiration in the field. Estimated transpiration of *Opuntia ficus-indica* during the growing season was similar to observations of daily average orchard transpiration rate of approximately 1.8 mm d^{-1} (Consoli et al., 2013; Goldstein et al., 1991). Dry biomass productivity values measured in the field for *O. ficus-indica* range from 1.3-5.0 kg m^{-2} yr^{-1} (Acevedo et al., 1983; Consoli et al., 2013; Cortazar & Nobel, 1990; de Cortázar & Nobel, 1992; Nobel et al., 1992; Nobel, 1991). Predicted values of productivity in the top *Opuntia* sp. producing regions lie within this range, with the exception of predicted potential productivity of 6.4 kg m^{-2} yr^{-1} in Mekele, Ethiopia. The expected biomass productivity predicted by this approach was similar to that derived using the established EPI in locations where the EPI model has been previously validated. Under certain environmental conditions, however, the model results diverged significantly. These conditions involved the presence of either relatively low PAR during the primary growing season, or rainfall patterns which were characterized by long periods of drought interspersed by small, intermittent rainfall events.

509 The discrepancy between the process based and empirical modeling approaches under low PAR
510 conditions may be explained by issues of scaling encountered when averaging environmental
511 conditions over long (monthly) timescales. Empirical modeling approaches currently estimate
512 CAM productivity as a function of monthly averaged environmental conditions, including solar
513 radiation (Nobel, 1988). Due to the strongly nonlinear response of photosynthetic rate to PAR
514 (see Fig. 2b) the same average monthly PAR will have a different effect on productivity
515 depending on how it is distributed across intra- and inter-daily timescales (which in turn will
516 vary depending on latitude and cloud cover patterns). Indeed, there is a known underestimation
517 of winter net assimilation rate observed in results from the EPI model, and it has been
518 hypothesized that this underestimation is due to using monthly PAR averages, rather than daily
519 PAR values (de Cortazar et al., 1985). Such underestimation likely extends to other situations,
520 seasonally and geographically, where light is a strong limiting factor on CAM productivity. This
521 is particularly relevant for many locations in the Eastern Hemisphere, for example in the
522 Mediterranean region and Northern Africa. The locations where the EPI was originally validated,
523 including Mexico, Chile, and the Southwestern United States, all tend to have high PAR
524 intensities during the main growing season (50-65 mol m^{-2} d^{-1}), creating circumstances under
525 which the averaging effect may not observed.
526
527 Discrepancies between the process based and empirical modeling approaches also arose under
528 certain rainfall patterns characterized by small, intermittent rainfall events. While the EPI
529 productivity estimates under such rainfall regimes were similar to estimates under well-watered
530 conditions, estimates of productivity calculated using the Photo3 model under these regimes
531 were significantly lower than well-watered estimates (see Fig. 7c and Fig. S3). This is most

likely due to the temporal dynamics of plant water storage and its impacts on CAM productivity. CAM crops such as *Opuntia* sp. and *Agave* sp. have a large amount of available water storage volume in the cladode and stem tissue (Goldstein et al., 1991; Nerd et al., 1991; Smith et al., 1987). Given the relatively shallow rooting depth of these plants (Park et al., 1986; Snyman, 2005), this stored water is significant when compared to the stored water in the soil and may easily be on the same order of magnitude (assuming typical values of 30 cm rooting depth, soil porosity of 0.4, plant water storage of 4 mm per unit leaf area, and a LAI of 3 yields a 1:1 ratio of plant to soil water storage). As a result, plant water stress is a function not only of the current available soil moisture and drought length, but is also strongly affected by plant hydration status, which depends on long-term soil moisture history (Hartzell et al., 2017; Huang et al., 2017; Kennedy et al., 2019). The effect of plant water storage is particularly pronounced when conditions of high soil moisture are unpredictable, infrequent, and brief (Holbrook, 1995). When small, intermittent rainfall events occur, the soil moisture may increase above the drought threshold without full recharge of plant water storage. In such a situation productivity during the subsequent drydown would be less than the productivity during a drydown which follows a long period of high soil moisture levels. Thus, in addition to total drought duration, the timing and depth of rainfall events at the daily scale are important in determining plant water stress. Inclusion of plant water storage in the modeling framework allows these effects to be taken into account.

Recent modeling efforts have addressed a range of questions regarding global CAM potential for agriculture and bioenergy using the EPI (Cortazar & Nobel, 1990; Owen & Griffiths, 2014; Yang et al., 2015). While useful and of widespread adoption, it is not based in plant physiology as are

555 many models of C3 and C4 crops (de Wit et al., 2018; Pachepsky & Acock, 1996; Tao et al.,
556 2009; Van Laar et al., 2005). Moreover, it is not clear that this method, which was developed and
557 calibrated under a limited set of environmental conditions, will transfer well to unfamiliar field
558 conditions. To date, the EPI model has been validated in a limited number of field sites in the
559 Americas (the Southwest US, Mexico, and Chile), while interest in CAM productivity is strong
560 in many disparate areas including North Africa, Europe, and Australia, which have very different
561 growing conditions. Models which are developed on a more mechanistic basis, like the one
562 presented here, are more likely to transfer successfully to novel conditions without requiring
563 recalibration. Similarly, while new environmental productivity indices must be developed for
564 each individual CAM species through labor-intensive field experiments, the grounding of this
565 modeling approach in basic principles may allow it to be applied to new species through the
566 adjustment of a small number of parameters which may be derived from laboratory experiments.
567
568 The results from this study suggest that previous predictions of global CAM potential may be a
569 significant underestimate in the Eastern Hemisphere, particularly under well-watered or irrigated
570 conditions. In Italy, Morocco, and Ethiopia, estimates of well-watered productivity calculated
571 using the Photo3 model and supported by field results were 30-40% higher than estimates
572 calculated using the EPI. Given that these regions together represent more than 300,000 ha of
573 current *Opuntia* sp. cultivation area (Inglese et al., 2017), current CAM potential could be
574 underestimated by hundreds of thousands of tons, a figure which would be amplified when
575 factoring in future planting area. Along with more accurate estimates of productivity potential,
576 predictions of CAM transpiration and water use efficiency may aid in deciding when and where
577 to plant such crops, informing irrigation strategies, and performing cost-benefit analyses for

578 CAM species. This extended modeling approach, grounded in physical principles, offers a
579 promising method for estimating CAM potential on a plot scale and globally.

Acknowledgments

This work was supported through the USDA Agricultural Research Service cooperative agreement 58-6408-3-027 and National Institute of Food and Agriculture (NIFA) grant 12110061; National Science Foundation (NSF) grants EAR-1331846, FESD- 1338694, EAR-1316258, and GRFP-1106401; the Carbon Mitigation Initiative (CMI) at Princeton University; the AFRI Postdoctoral Fellowship program Grant No. 2017-67012-26106/project accession Number 1011029 from the USDA National Institute of Food and Agriculture; and the National Natural Science Foundation of China (41877158, 51739009).

603 **References**

604

605 Acevedo, E., Badilla, I., & Nobel, P. S. (1983). Water relations, diurnal acidity changes, and
606 productivity of a cultivated cactus, Opuntia ficus-indica. *Plant Physiology*, *72*(3), 775–780.
607 Amthor, J. S. (1994). Plant responses to the environment and their effects on the carbon balance.
608 In R. E. Wilkinson (Ed.), *Plant Environment Interactions* (pp. 501–554).
609 Arba, M., Benismail, M. C., & Mokhtari, M. (2002). Cactus pear (Opuntia spp.) in Morocco:
610 main species and cultivar characterization. *Acta Horticulturae*, (581), 103–109.
611 Arba, Mohamed, Falisse, A., Choukr-Allah, R., & Sindic, M. (2017). Biology, flowering and
612 fruiting of the Cactus opuntia spp.: A review and some observations on three varieties in
613 Morocco. *Brazilian Archives of Biology and Technology*, *60*, 1–11.
614 Bartlett, M. S., Vico, G., & Porporato, A. (2014). Coupled carbon and water fluxes in CAM
615 photosynthesis: modeling quantification of water use efficiency and productivity. *Plant and*
616 *Soil*, *383*(1–2), 111–138.
617 Blasius, B., Neff, R., Beck, F., & Lüttge, U. (1999). Oscillatory model of crassulacean acid
618 metabolism with a dynamic hysteresis switch. *Proceedings of the Royal Society B:*
619 *Biological Sciences*, *266*, 93–101.
620 Borland, A. M., Griffiths, H., Hartwell, J., & Smith, J. A. C. (2009). Exploiting the potential of
621 plants with crassulacean acid metabolism for bioenergy production on marginal lands.
622 *Journal of Experimental Botany*, *60*(10), 2879–2896.
623 Boujghagh, M., & Bouharroud, R. (2015). Influence of the timing of flowers and young cladodes
624 removal on reflowering and harvest periods, yields and fruits quality of prickly pear
625 (Opuntia ficus-indica). *Acta Horticulturae*, *1067*, 79–82.
626 Conde, L. F., & Kramer, P. J. (2008). The effect of vapor pressure deficit on diffusion resistance

627 in Opuntia compressa. *Canadian Journal of Botany*, *53*(24), 2923–2926.
628 Consoli, S., Inglese, G., & Inglese, P. (2013). Determination of evapotranspiration and annual
629 biomass productivity of a cactus pear [Opuntia ficus-indica L. (Mill.)] orchard in a semi-
630 arid environment. *Journal of Irrigation and Drainage Engineering*, *139*(8), 680–690.
631 Cui, M., & Nobel, P. S. (1994). Gas exchange and growth responses to elevated CO_2 and light
632 levels in the CAM species Opuntia ficus-indica. *Plant, Cell & Environment*, *17*(8), 935–
633 944.
634 Cui, Muyi, Miller, P. M., & Nobel, P. S. (1993). CO_2 Exchange and Growth of the Crassulacean
635 Acid Metabolism Plant Opuntia ficus-indica under Elevated CO_2 in Open-Top Chambers.
636 *Plant Physiology*, *103*(2), 519–524.
637 Daly, E., Porporato, A., & Rodriguez-Iturbe, I. (2004). Coupled dynamics of photosynthesis,
638 transpiration, and soil water balance. Part I: Upscaling from hourly to daily level. *Journal of*
639 *Hydrometeorology*, *5*(3), 546–558.
640 de Cortazar, V. G., Acevedo, E., & Nobel, P. S. (1985). Modeling of PAR interception and
641 productivity by Opuntia ficus-indica. *Agricultural and Forest Meteorology*, *34*(2–3), 145–
642 162.
643 de Cortazar, V. G., & Nobel, P. S. (1990). Worldwide environmental productivity indices and
644 yield predictions for a CAM plant, Opuntia ficus-indica, including effects of doubled CO_2
645 levels. *Agricultural and Forest Meteorology*, *49*, 261–279.
646 de Cortázar, V. G., & Nobel, P. S. (1992). Biomass and Fruit Production for the Prickly Pear
647 Cactus, Opuntia ficus-indica. *Journal of the American Society for Horticultural Science*,
648 *117*(4), 558–562.
649 de Wit, A., van Kraalingen, D., Supit, I., van der Wijngaart, R., Janssen, S., van Diepen, K., …

650 Fumagalli, D. (2018). 25 years of the WOFOST cropping systems model. *Agricultural*
651 *Systems*, *168*, 154–167.
652 Drennan, P. M., & Nobel, P. S. (1998). Root growth dependence on soil temperature for Opuntia
653 ficus-indica: influences of air temperature and a doubled CO_2 concentration. *Functional*
654 *Ecology*, *12*(6), 959–964.
655 Dubeux, J. C. B., dos Santos, M. V. F., de Andrade Lira, M., dos Santos, D. C., Farias, I., Lima,
656 L. E., & Ferreira, R. L. C. (2006). Productivity of Opuntia ficus-indica (L.) Miller under
657 different N and P fertilization and plant population in north-east Brazil. *Journal of Arid*
658 *Environments*, *67*(3), 357–372.
659 Farquhar, G. D., von Caemmerer, S., & Berry, J. A. (1980). A biochemical model of
660 photosynthetic CO_2 assimilation in leaves of C3 species. *Planta*, *149*, 78–90.
661 Gebretsadik, G., Animut, G., & Tegegne, F. (2013). Assessment of the potential of cactus pear
662 (Opuntia ficus indica) as livestock feed in Northern Ethiopia. *Livestock Research for Rural*
663 *Development*, *25*(2), 1–11.
664 Geller, G., & Nobel, P. S. (1987). Comparative cactus architecture and PAR interception.
665 *American Journal of Botany*, *74*(7), 998–1005.
666 Goldstein, G., Andrade, J. L., & Nobel, P. S. (1991). Differences in water relations parameters
667 for the chlorenchyma and the parenchyma of Opuntia ficus-indica under wet versus dry
668 conditions. *Australian Journal of Plant Physiology*, *18*(2), 95–107.
669 Goldstein, G., Ortega, J. K. E., Nerd, A., & Nobel, P. S. (1991). Diel Patterns of Water Potential
670 Components for the Crassulacean Acid Metabolism Plant Opuntia ficus-indica when Well-
671 Watered or Droughted. *Plant Physiology*, *95*(1), 274–280.
672 Hartzell, S., Bartlett, M. S., & Porporato, A. (2017). The role of plant water storage and

673 hydraulic strategies in relation to soil moisture availability. *Plant and Soil*, *419*, 503–521.
674 Hartzell, S., Bartlett, M. S., & Porporato, A. (2018). Unified representation of the C3, C4, and
675 CAM photosynthetic pathways with the Photo3 model. *Ecological Modelling*, *384*, 173–
676 187.
677 Hartzell, S., Bartlett, M. S., Virgin, L., & Porporato, A. (2015). Nonlinear dynamics of the CAM
678 circadian rhythm in response to environmental forcing. *Journal of Theoretical Biology*, *368*,
679 Holbrook, N. M. (1995). Stem Water Storage. In Barbara Gartner (Ed.), *Plant Stems* (pp. 151–
680 174). Academic Press.
681 Huang, C. W., Domec, J. C., Ward, E. J., Duman, T., Manoli, G., Parolari, A. J., & Katul, G. G.
682 (2017). The effect of plant water storage on water fluxes within the coupled soil-plant
683 system. *New Phytologist*, *213*(3), 1093–1106.
684 Inglese, P., Inglese, G., & Liguori, G. (2012). Fruit productivity and carbon gain of Opuntia
685 ficus-indica (L.) Mill. trees. *Israel Journal of Plant Sciences*, *60*, 283–289.
686 Inglese, P., Mondragon, C., Nefzaoui, A., & Saenz, C. (2017). *Crop ecology, cultivation, and*
687 *uses of cactus pear*. (P. Inglese, C. Mondragon, A. Nefzaoui, & C. Saenz, Eds.), *Crop*
688 *Ecology, Cultivation and Uses of Catus Pears*. Food and Agriculture Organization of the
689 United Nations.
690 Iñiguez-Covarrubias, G., Díaz-Teres, R., Sanjuan-Dueñas, R., Anzaldo-Hernández, J., & Rowell,
691 R. M. (2001). Utilization of by-products from the tequila industry. Part 2: Potential value of
692 Agave tequilana Weber azul leaves. *Bioresource Technology*, *77*(2), 101–108.
693 Jones, H. G. (2014). *Plants and microclimate: A quantitative approach to plant physiology*.
694 Cambridge, United Kingdom: Cambridge University Press.
695 Katul, G. G., Palmroth, S., & Oren, R. (2009). Leaf stomatal responses to vapour pressure deficit

under current and CO_2-enriched atmosphere explained by the economics of gas exchange. *Plant, Cell and Environment*, *32*, 968–979.

Kennedy, D., Swenson, S., Oleson, K. W., Lawrence, D. M., Fisher, R., Lola da Costa, A. C., & Gentine, P. (2019). Implementing plant hydraulics in the Community Land Model, Version 5. *Journal of Advances in Modeling Earth Systems*, *11*(2), 485–513.

Kluge, M., & Ting, I. P. (1978). *Crassulacean acid metabolism: Analysis of an ecological adaptation*. (W. D. Billings & O. L. Lange, Eds.). New York: Springer-Verlag.

Lambers, H., Stuart Chapin III, F., & Pons, T. L. (2008). *Plant physiological ecology*. Springer.

Lange, O. L., & Medina, E. (1979). Stomata of the CAM plant Tillandsia recurvata respond directly to humidity. *Oecologia*, *40*(3), 357–363.

Leuning, R. (1995). A critical appraisal of a combined stomatal-photosynthesis model for C3 plants. *Plant, Cell and Environment*, *18*(4), 339–355.

Liguori, G., Inglese, P., Sortino, G., & Inglese, G. (2014). Dry matter accumulation and seasonal partitioning in mature Opuntia ficus-indica (L.) Mill. fruiting trees. *Italian Journal of Agronomy*, *9*(1), 44–47.

Linton, M. J., & Nobel, P. S. (2001). Hydraulic conductivity, xylem cavitation, and water potential for succulent leaves of Agave deserti and Agave tequilana. *International Journal of Plant Sciences*, *162*(4), 747–754.

Males, J., & Griffiths, H. (2017). Stomatal biology of CAM plants. *Plant Physiology*, *174*, 550-560.

Mason, P. M., Glover, K., Smith, J. A. C., Willis, K. J., Woods, J., & Thompson, I. P. (2015). The potential of CAM crops as a globally significant bioenergy resource: moving from `fuel or food' to `fuel and more food'. *Energy and Environmental Science*, *8*, 2320–2329.

719 Medlyn, B. E., Duursma, R. A., Eamus, D., Ellsworth, D. S., Prentice, I. C., Barton, C. V. M., …
720 Wingate, L. (2011). Reconciling the optimal and empirical approaches to modelling
721 stomatal conductance. *Global Change Biology*, *17*(6), 2134–2144.
722 Menezes, R. S. C., Simoes, D. A., & Sampaio, E. V. S. (2005). *A palma no Nordeste do Brasil*.
723 Recife, Brazil.
724 Morales, F., Pavlovič, A., Abadía, A., & Abadía, J. (2018). Photosynthesis in poor nutrient soils,
725 in compacted soils, and under drought. In *The Leaf: A Platform for Performing*
726 *Photosynthesis* (pp. 371–399). Springer.
727 Nerd, A., Karadi, A., & Mizrahi, Y. (1991). Salt tolerance of prickly pear cactus (Opuntia ficus-
728 indica). *Plant and Soil*, *137*, 201–207.
729 Niechayev, N. A., Jones, A. M., Rosenthal, D. M., & Davis, S. C. (2018). A model of
730 environmental limitations on production of Agave americana L. grown as a biofuel crop in
731 semi-arid regions. *Journal of Experimental Botany*, 1–11.
732 Nobel, P.S., Alm, D. M., & Cavelier, J. (1992). Growth respiration, maintenance respiration and
733 structural-carbon costs for roots of three desert succulents. *Functional Ecology*, *6*(1), 144–
734 151.
735 Nobel, Park S. (1985). PAR, water, and temperature limitations on the productivity of cultivated
736 Agave fourcroydes (Henequen). *British Ecological Society*, *22*(1), 157–173.
737 Nobel, Park S. (1988). *Environmental biology of agaves and cacti*. Cambridge: Cambridge
738 University Press.
739 Nobel, Park S. (1989). A nutrient index quantifying productivity of agaves and cacti. *Journal of*
740 *Applied Ecology*, *26*(2), 635–645.
741 Nobel, Park S. (1991). Achievable productivities of certain CAM plants: basis for high values

742 compared with C3 and C4 plants. *New Phytologist*, *119*(2), 183–205.
743 Nobel, Park S., & Hartsock, T. L. (1983). Relationships between photosynthetically active
744 radiation, nocturnal acid accumulation, and CO_2 uptake for a Crassulacean Acid
745 Metabolism plant, Opuntia ficus-indica. *Plant Physiology*, *71*(1), 71–75.
746 Nobel, Park S., & Hartsock, T. L. (1986). Environmental influences on the productivity of three
747 desert succulents in the south-western United States. *Plant, Cell and Environment*, *9*, 741–
748 749.
749 Nobel, Park S., & Jordan, P. W. (1983). Transpiration stream of desert species: resistances and
750 capacitances for a C3, a C4 and a CAM plant. *Journal of Experimental Botany*, *34*(147),
751 1379–1391.
752 Nobel, Park S., & Meyer, S. E. (1985). Field productivity of a CAM plant, Agave salmiana,
753 estimated using daily acidity changes under various environmental conditions. *Physiologia*
754 *Plantarium*, *65*(4), 397–404.
755 Nobel, Park S., & Quero, E. (1986). Environmental Productivity Indices for a Chihuahuan Desert
756 CAM Plant , Agave Lechuguilla. *Ecological Society of America*, *67*(1), 1–11.
757 Nobel, Park S., & Valenzuela, A. G. (1987). Environmental responses and productivity of the
758 CAM plant, Agave tequilana. *Agricultural and Forest Meteorology*, *39*(4), 319–334.
759 Norman, J. M. (1982). Simulation of microclimates. In *Biometeorology in integrated pest*
760 *management* (pp. 65–99).
761 Oren, R., Sperry, J. S., Katul, G. G., Pataki, D. E., Ewers, B. E., Phillips, N., & Schäfer, K. V. R.
762 (1999). Survey and synthesis of intra- and interspecific variation in stomatal sensitivity to
763 vapour pressure deficit. *Plant, Cell and Environment*, *22*(12), 1515–1526.
764 Osmond, C. B., Ludlow, M. M., Davis, R., Cowan, I. R., Powles, S. B., Winter, K., & Dawis, R.

765 (1979). Stomatal responses to humidity in Opuntia inermis in relation to control of CO_2 and
766 H_2O exchange patterns. *Oecologia*, *41*(1), 65–76.
767 Owen, N. A., Choncubhair, Ó. N., Males, J., del Real Laborde, J. I., Rubio-Cortés, R., Griffiths,
768 H., & Lanigan, G. (2016). Eddy covariance captures four-phase crassulacean acid
769 metabolism (CAM) gas exchange signature in Agave. *Plant Cell and Environment*, *39*(2),
770 295–309.
771 Owen, N. A., & Griffiths, H. (2014). Marginal land bioethanol yield potential of four
772 crassulacean acid metabolism candidates (Agave fourcroydes, Agave salmiana, Agave
773 tequilana and Opuntia ficus-indica) in Australia. *GCB Bioenergy*, *6*(6), 687–703.
774 Owen, N., & Griffiths, H. (2013). A system dynamics model integrating physiology and
775 biochemical regulation predicts extent of crassulacean acid metabolism (CAM) phases. *New*
776 *Phytologist*, *200*(4), 1116–1131.
777 Pachepsky, L. B., & Acock, B. (1996). A model 2DLEAF of leaf gas exchange: Development,
778 validation, and ecological application. *Ecological Modelling*, *93*(1–3), 1–18.
779 Palta, J. A., & Nobel, P. S. (1989). Influences of water status, temperature, and root age on daily
780 patterns of root respiration for two cactus species. *Annals of Botany*, *63*(6), 651–662.
781 Shameer, S., Baghalian, K., Cheung, C. Y. M., Ratcliffe, R. G., & Sweetlove, L. J. (2018).
782 Computational analysis of the productivity potential of CAM. *Nature Plants*, *4*(3), 165–171.
783 Skillman, J. B. (2008). Quantum yield variation across the three pathways of photosynthesis: Not
784 yet out of the dark. *Journal of Experimental Botany*, *59*(7), 1647–1661.
785 Smith, J. A. C., Schulte, P. J., & Nobel, P. S. (1987). Water flow and water storage in Agave
786 deserti: osmotic implications of crassulacean acid metabolism. *Plant, Cell and*
787 *Environment*, *10*(8), 639–648.

788 Snyman, H. A. (2005). A case study on in situ rooting profiles and Water-Use Efficiency of
789 cactus pears, Opuntia ficus-indica and O. robusta. *Journal for the Professional Association*
790 *for Cactus Development*, *7*, 1–21.
791 Tao, F., Yokozawa, M., & Zhang, Z. (2009). Modelling the impacts of weather and climate
792 variability on crop productivity over a large area: A new process-based model development,
793 optimization, and uncertainties analysis. *Agricultural and Forest Meteorology*, *149*(5), 831–
794 850.
795 Tcherkez, G. (2017). Respiratory Metabolism in CAM Plants. In G. Tcherkez & J. Ghashghaie
796 (Eds.), *Plant respiration: metabolic fluxes and carbon balance* (pp. 227–246). Springer.
797 Van Laar et al. (2005). *Crop systems dynamics: an ecophysiological simulation model for*
798 *genotype-by-environment interactions*. Wageningen Academic Publishers.
799 Weng, E. S., Malyshev, S., Lichstein, J. W., Farrior, C. E., Dybzinski, R., Zhang, T., … Pacala,
800 S. W. (2014). Scaling from individuals to ecosystems in an Earth System Model using a
801 mathematically tractable model of height-structured competition for light. *Biogeosciences*
802 *Discussions*, *11*(12), 17757–17860.
803 Wilkins, M. B. (1992). Circadian rhythms: their origin and control. *New Phytologist*, *121*(3),
804 347–375.
805 Winter, K., & Smith, J. A. C. (Eds.). (1996). *Crassulacean acid metabolism: Biochemistry,*
806 *ecophysiology and evolution*. *Ecological Studies* (Vol. 114). Springer-Verlag Berlin
807 Heidelberg.
808 Woodhouse, R. M., Williams, J. G., & Nobel, P. S. (1980). Leaf orientation, radiation
809 interception, and nocturnal acidity increases by the CAM plant Agave deserti (Agavaceae).
810 *American Journal of Botany*, *67*(8), 1179–1185.

Yang, X., Cushman, J. C., Borland, A. M., Edwards, E. J., Wullschleger, S. D., Tuskan, G. A., … Holtum, J. A. M. (2015). A roadmap for research on crassulacean acid metabolism (CAM) to enhance sustainable food and bioenergy production in a hotter, drier world. *New Phytologist*, *207*, 491–504.

Tables

Table 1: Plant Parameters

Parameter	*O. ficus-indica*	*A. tequilana*	Units	Description
V_{cmax}	18[a]	19.5[b]	μ mol m^{-2} s^{-1}	Maximum carboxylation capacity
J_{max}	36[a]	39[b]	μ mol m^{-2} s^{-1}	Maximum electron transport rate
M_{max}	230[a]	130[b]	mol m^{-3}	Maximum malic acid concentration
$A_{m,max}$	14[a]	11.1[b]	µmol m^{-2} s^{-1}	Maximum rate of malic acid storage flux
LAI	3.5[c]	6[d]	m^2 m^{-2}	Leaf area index
Z_r	0.3	0.3	m	Rooting depth
f_{PAR}	0.58[e]	0.3[e]	-	PAR interception factor
r_r	0.14[f]	0.11[d]	-	Partitioning to roots
r_l	0.63[c]	0.65[d]	-	Partitioning to leaves (photosynthetically active cladodes)
r_s	0.12[c]	0.1[d]	-	Partitioning to stem (lignified cladodes)
r_o	0.25[c,g]	0.14[d]	-	Partitioning to storage organs (fruit)
b_o	66[h]	48[i]	mol C m^{-2} leaf area	Initial biomass
η_g	0.2	0.2	-	Growth respiration coefficient
T_L	278[i]	278[i]	K	Thermal inhibition low temperature
T_H	318[j]	318[j]	K	Thermal inhibition high temperature
Z_w	11.3	4.15[l]	mm	Maximum depth of water stored per unit leaf area
c	0.83	0.27[m]	MPa^{-1}	Intrinsic plant hydraulic capacitance

[a]Calculated using data from Nobel and Hartsock (1983)

822 [b]Nobel & Valenzuela (1987)

823 [c]Consoli et al. (2013)

824 [d]Nobel & Valenzuela (1987)

825 [e]Calculated in 2.3. *PAR interception*

826 [f]Drennan & Nobel (1998); Liguori et al. (2014)

827 [g]Acevedo et al. (1983)

828 [h]Following Liguori et al. (2014), assumed to be about three times the annual productivity

829 [i]Following Nobel & Valenzuela (1987)

830 [j] Weng et al. (2014)

831 [k]Based on Goldstein, Andrade, & Nobel (1991)

832 [l]Value is 62% of the value for *Agave deserti* based on the size difference (Linton & Nobel, 2001;

833 Nobel & Jordan, 1983)

834 [m]Based on observation for *Agave deserti* following Nobel & Jordan (1983)

835

Figures

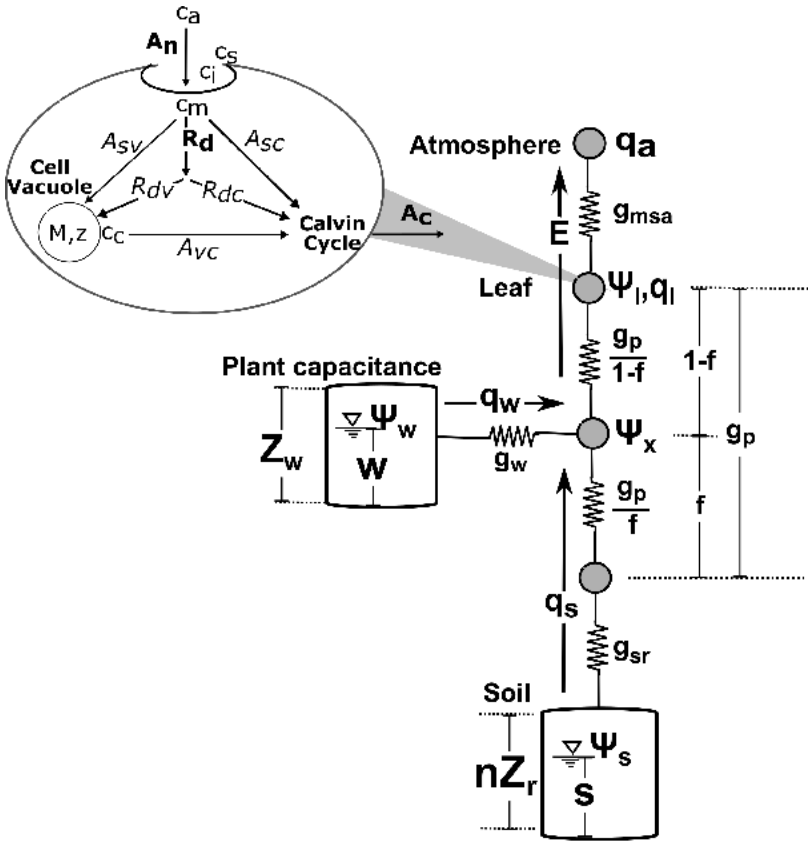

Figure 1: The Photo3 model depicts the CAM circadian rhythm of malic acid storage and release coupled to the soil-plant-atmosphere continuum to predict CAM carbon assimilation and water use on an hourly timescale. After Bartlett et al. (2014).

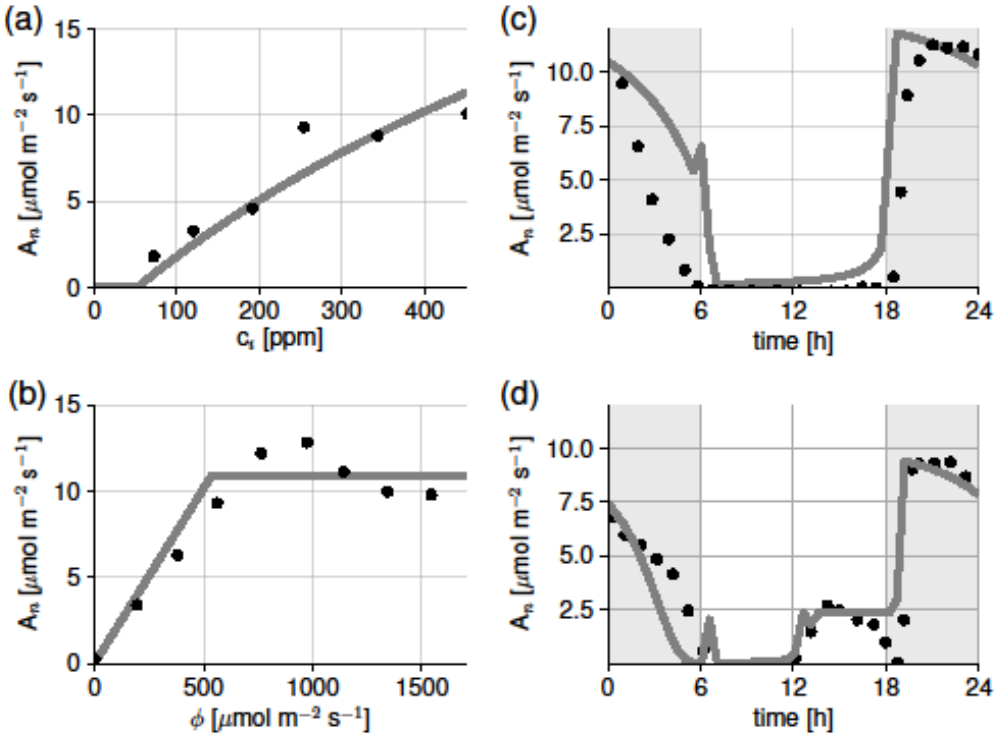

Figure 2: Modeled response (solid line) of net carbon assimilation, A_n to (a) internal CO_2 concentration, c_i, and (b) photosynthetically active radiation, ϕ, for *Opuntia ficus-indica*. Data (filled circles) on response to CO_2 from Osmond et al. (1979) and on response to light from Nobel & Hartsock (1983). Simulations of net carbon assimilation (solid line) for (c) *O. ficus-indica* and (d) *Agave tequilana* compared with data (filled circles) from Nobel & Hartsock (1983) and Nobel & Valenzuela, (1987), respectively. In (c), environmental inputs were T_a = 25 C, RH = 40%, ϕ = 244 W m^{-2} (light period); T_a = 15 C, RH = 60%, ϕ = 0 W m^{-2} (dark period) while in (d), environmental inputs were T_a = 30 C, RH = 33%, ϕ = 200 W m^{-2} (light period); T_a = 15 C, RH = 78%, ϕ = 0 W m^{-2} (dark period). Shaded bars represent dark hours.

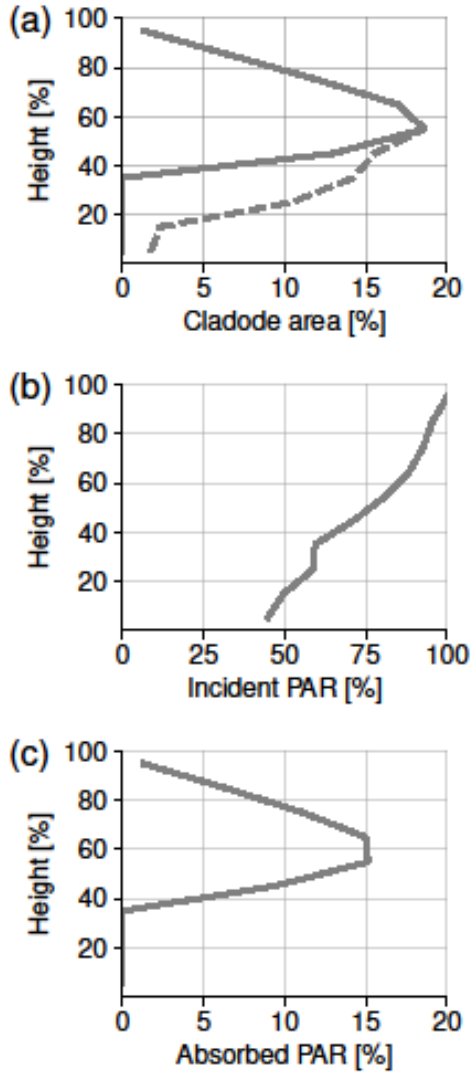

853

854 **Figure 3:** Calculation of photosynthetically active radiation (PAR) interception for *Opuntia*
855 *ficus-indica*. (a) Cladode area distribution with height (de Cortazar et al., 1985), where the lower
856 30% of cladode area is assumed to be lignified (dotted line). (b) Incident PAR distribution with
857 height (de Cortazar et al., 1985). (c) The absorbed PAR is the product of the relative unlignified
858 cladode area and the relative incident PAR.

859

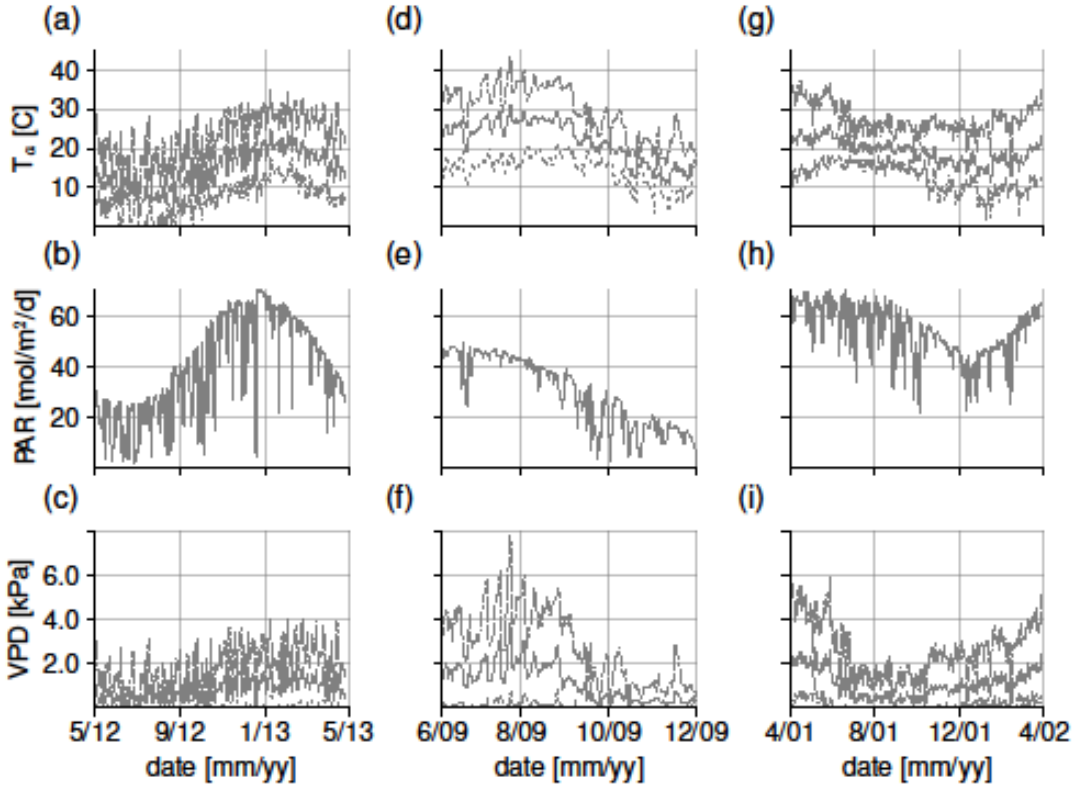

860

861 **Figure 4:** Daily (a) temperature, T_a, (b) photosynthetically active radiation (PAR), and (c) vapor
862 pressure deficit (VPD) for La Platina, Chile, growing season 2012-13; (d) temperature, (e) PAR,
863 and (f) VPD for Roccapalumba, Italy, growing season 2009; (g) temperature, (h) PAR, and (i)
864 VPD for Jalisco, Mexico, 2001-2002. Solid lines correspond to daily averages, dashed lines
865 correspond to daily maximum values, and dotted lines correspond to daily minimum values.

866

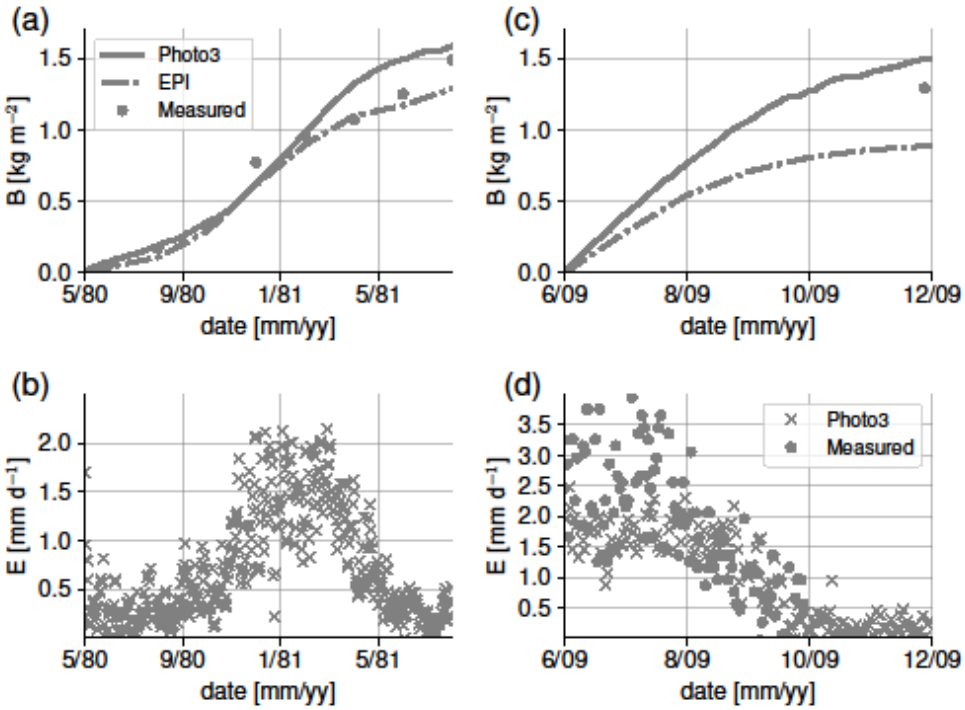

867

868 **Figure 5:** Simulated (a) aboveground dry biomass gain per unit stem area (B) according to the
869 presented (Photo3) and empirical (EPI) models with field data from (de Cortazar et al., 1985), (b)
870 daily transpiration per unit ground area (E) according to the Photo3 model for *Opuntia ficus-*
871 *indica* in Til Til, Chile; (c) aboveground dry biomass gain per unit ground area (B) according to
872 the Photo3 and EPI models with data from (Consoli et al., 2013), (d) daily transpiration per unit
873 ground area (E) according to the Photo3 model for *O. ficus-indica* in Roccapalumba, Italy.

874

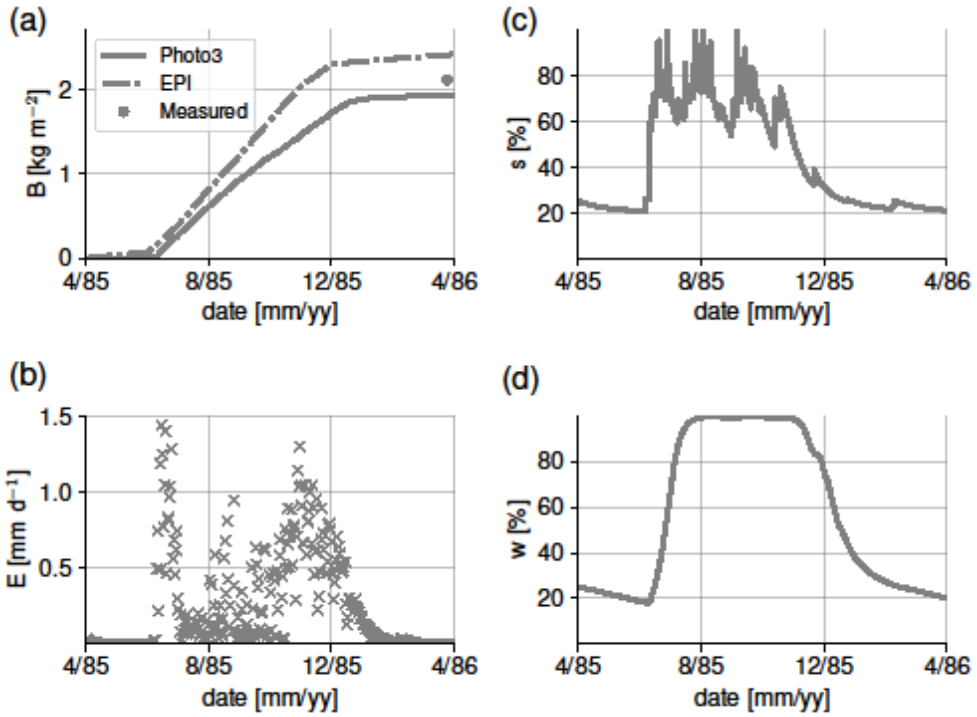

875

876 **Figure 6:** Simulated (a) aboveground dry biomass gain per unit ground area (B) according to the
877 presented (Photo3) and empirical (EPI) models with data from Nobel & Valenzuela (1987) (b)
878 daily transpiration per unit ground area (E) according to the Photo3 model, (c) plant water
879 content, and (d) soil moisture for *Agave tequilana* in Jalisco, Mexico.

880

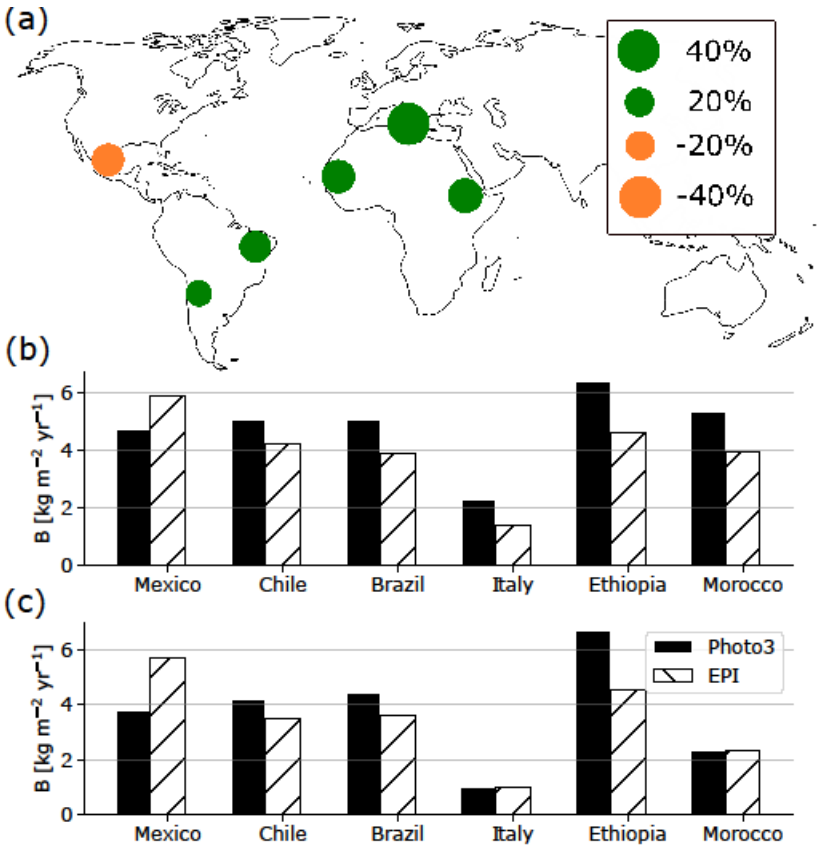

881

882 **Figure 7:** Photo3 and EPI model prediction for *Opuntia ficus-indica* aboveground dry mass
883 productivity in six regions of high *Opuntia* sp. productivity: Mexico City, Mexico; Til Til,
884 Chile; Serra Talhada, Brazil; Roccapalumba, Italy; Mekele, Ethiopia; Agadir, Morocco. (a)
885 percentage difference between Photo3 and EPI predictions under well-watered conditions; (b)
886 aboveground dry mass productivity per unit ground area under well-watered conditions; (c)
887 aboveground dry mass productivity per unit ground area under rainfed conditions.

888

889 **Supporting information figures**

890

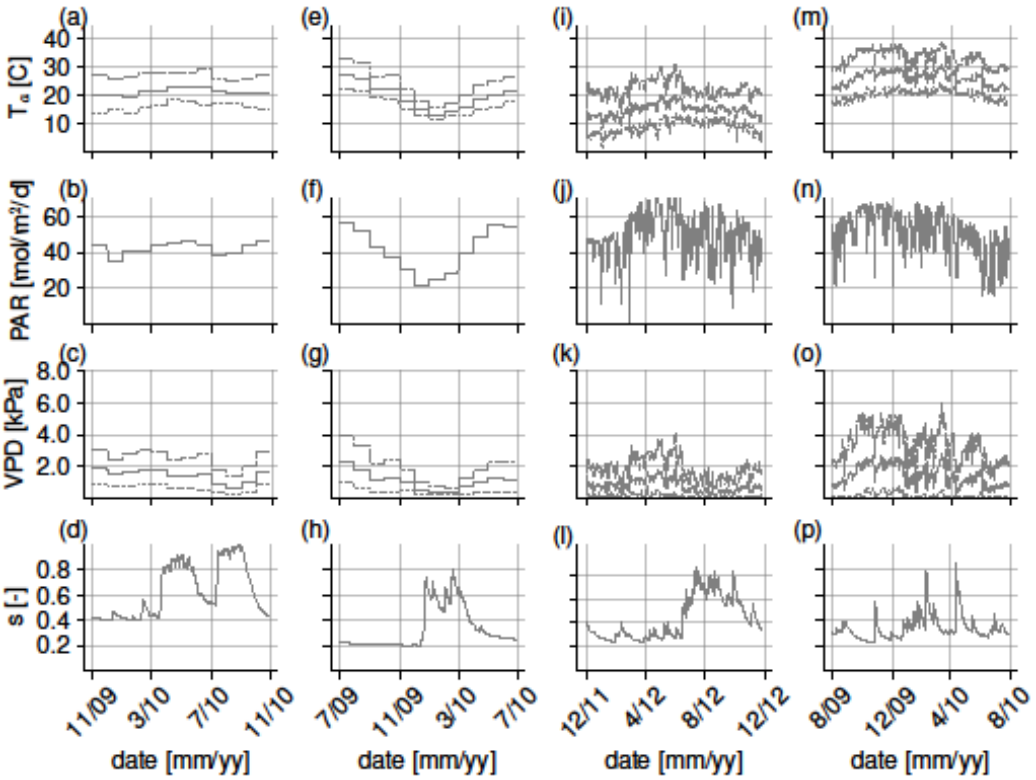

Figure S1. Temperature (T_a), photosynthetically active radiation (PAR), vapor pressure deficit (VPD), and soil moisture (s) in Mekele, Ethiopia (a, e, i, m); Agadir, Morocco (b, f, j, n); Mexico City, Mexico (c, g, k, o); and Serra Talhada, Brazil (d, h, l, p). Where relevant, daily maxima are indicated by a dot-dashed line, daily averages are indicated by a solid line, and daily minima are indicated by a dotted line.

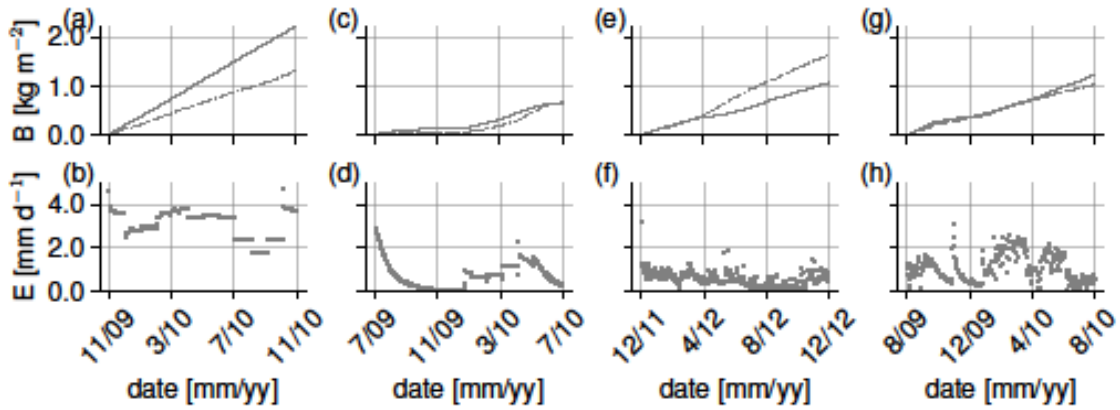

Figure S2. Photo3 (solid line) and EPI model (dot-dashed line) prediction for aboveground dry mass productivity (B) on a leaf area basis, and Photo3 prediction for transpiration (E) on a ground area basis for *Opuntia ficus-indica* in Mekele, Ethiopia (a, b); Agadir, Morocco (c, d); Mexico City, Mexico (e, f); and Serra Talhada, Brazil (g, h) under rainfed conditions.

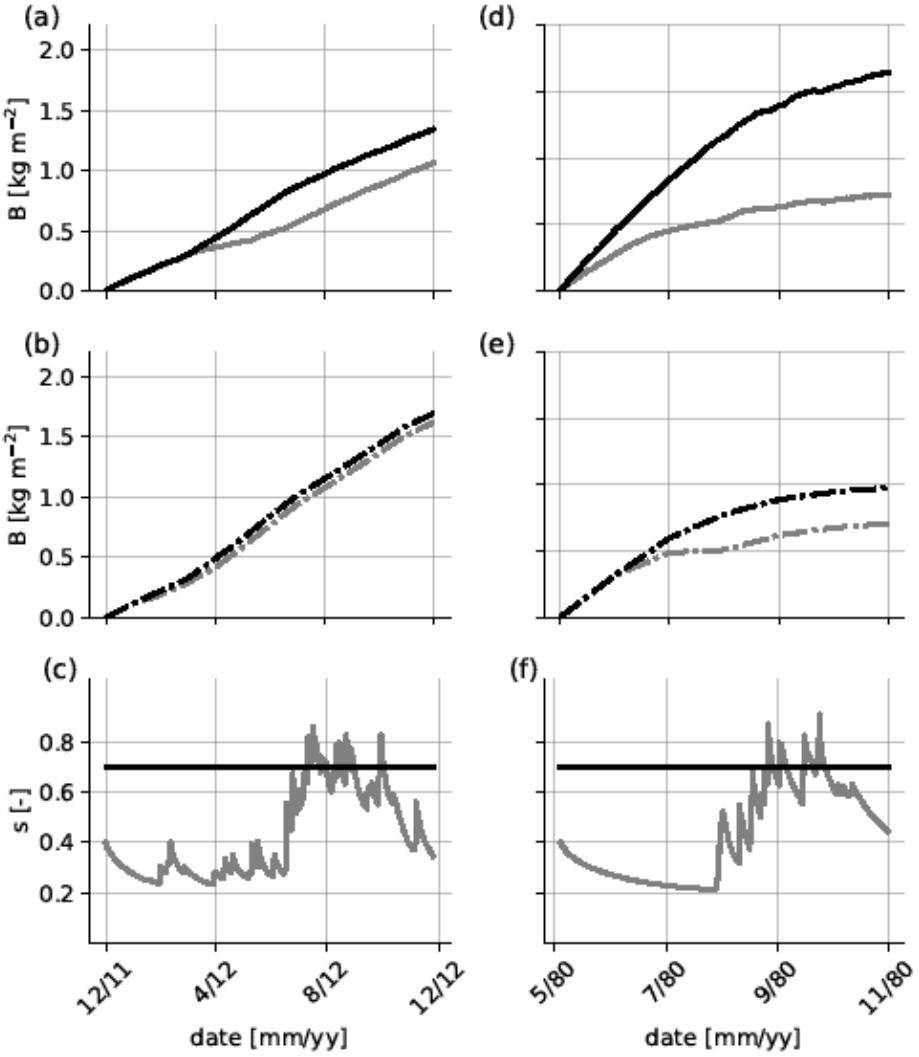

Figure S3. Total aboveground dry mass accumulation on a leaf area basis calculated using the Photo3 model (a, d, solid line) and the EPI model (b, e, dot-dashed line) under both well-watered (black line) and rainfed (grey line) conditions. (c, f) soil moisture input to each model under

well-watered and rainfed conditions. (a, b, c) are results in Roccapalumba, Italy, while (d, e, f) are results in Mexico City, Mexico.

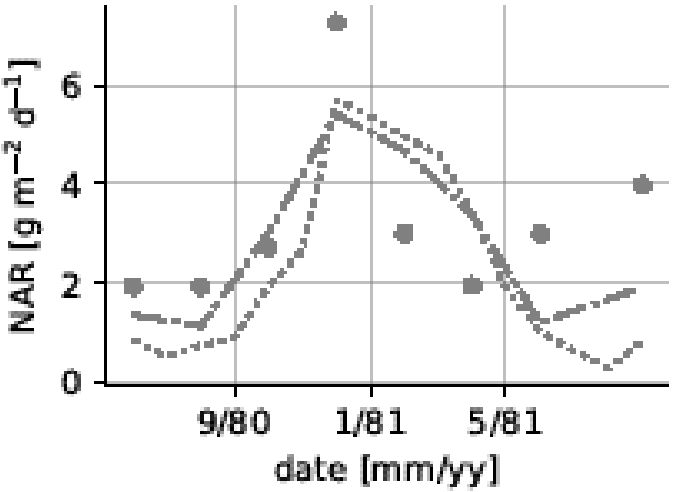

Figure S4. Net assimilation rate (NAR) based upon the EPI index calculated using 2012-2013 temperature, relative humidity, and solar radiation data from the La Platina station of the Chilean Institute of Agricultural Research (INIA) Agromet network (dotted line) and EPI index from the original study period (de Cortazar et al. 1985) (dashed line).